Symmetry Breaking in Seed-Mediated Silver Nanorod Growth Induced by Dimethyl Sulfoxide

Claire Goldmann, Marta de Frutos, Eric H Hill, Doru Constantin, Cyrille Hamon

Symmetry breaking in seed-mediated silver nanorod growth induced by dimethyl sulfoxide

Claire Goldmann,[1] Marta de Frutos,[1] Eric H. Hill,[2]* Doru Constantin,[1]* Cyrille Hamon[1]*

[1] Université Paris-Saclay, CNRS, Laboratoire de Physique des Solides, 91405 Orsay, France.

[2] Institute of Physical Chemistry, University of Hamburg, Grindelallee 117, 20146 Hamburg, Germany; The Hamburg Center for Ultrafast Imaging (CUI), Luruper Chausee 149, 22761 Hamburg, Germany

Abstract

Engineering symmetry breaking in seed-mediated growth is a fundamental challenge to produce colloidal nanocrystals with controlled morphologies and properties. In this work, we show a simple, aqueous approach to breaking the inversion symmetry of silver nanorods by restricting growth to one end of the pentatwinned gold bipyramid seed. Controlled addition of dimethyl sulfoxide (DMSO) allows us to tune both the symmetry and the length and width of the objects. Simulations and experiments demonstrate the adsorption of DMSO, which displaces interfacial water, reduces binding of surfactant and chloride ions at the gold surface, and slows down the deposition kinetics of silver. Besides showing the potential of DMSO for controlling the synthesis of complex nanostructures, this work opens new perspectives for the study of the physical properties of non-centrosymmetric nanoparticles, e.g. by controlling their plasmon modes and their second-harmonic generation efficiency.

Introduction

Bimetallic nanoparticles (NPs) composed of a gold core and a silver shell have gained increasing significance with respect to tailoring their localized surface plasmon resonance (LSPR), which can be adjusted by varying the morphology and composition of the bimetallic NPs.[1] Their synthesis is usually performed by seed-mediated growth: one first obtains gold nanoparticles (AuNPs), onto which the silver shell is grown in a second step.[2] Colloidal chemistry allows control of stacking fault formation in the structure of the seed, providing a convenient route for synthesizing anisotropic NPs.[3, 4] In such cases, silver is deposited in a way which minimizes strain in the NPs[5, 6] and the morphology of the final particles can also be modulated with molecular or ionic additives, such as ascorbic acid[7] or halides, respectively.[4, 8] For instance, in the presence of chloride ions silver grows on the high-index lateral facets of monocrystalline gold nanorods, yielding cuboidal Au@Ag NPs.[9-11] If the gold seeds are pentatwinned (stacking faults with five-fold symmetry along the long axis of the NP), silver grows along their fivefold axis and yields rod-like Au@Ag NPs.[6, 12]

Depositing Ag on pentatwinned gold bipyramids (AuBPs) is an efficient way of forming Ag nanorods (AgNRs) with a tunable aspect ratio, which can be increased significantly upon controlled Ag addition, shifting the LSPR from the visible to the infrared region.[12-14] Such nanostructures can sustain multiple plasmon modes, a useful feature for surface-enhanced spectroscopy applications.[12, 15, 16] Previous work reported the formation of AgNRs in which the AuBPs were located at the center of mass, but shifting the seed position within the nanorod has not yet been demonstrated.

It is challenging to control metal deposition on a gold seed in a way that would lead to the formation of non-centrosymmetric nanostructures. This can be achieved when there is a lattice mismatch between the elements used for the core and the shell, but these conditions are not met in the case of gold and silver due to their almost identical lattice constants.[17] It is also

possible to engineer interfacial stress with ligands such as thiolated molecules, but the high affinity of thiols to both gold and silver limits shape control in this case.[18, 19] Multistep approaches involving sacrificial masks have also been developed, but they are complex and time-consuming.[20-23] In this context, a more promising way to achieve precise morphological control is by manipulating the reduction kinetics in the seed-mediated growth process.[2, 24-26] For instance, asymmetric growth was achieved under kinetic control by modulating the injection rate of the metallic precursor solution.[24, 26, 27] In another example, the asymmetric growth of Ag on Au seeds was induced by modulating the Ag deposition rate via controlled addition of ammonia in a polyol process.[28]

Dimethyl sulfoxide (DMSO) is completely miscible in water and the micellization of surfactants in such mixtures is strongly modified with respect to pure water.[29-32] In general, the critical micelle concentration increases with the DMSO content, up to a threshold value above which no micelles form. Since surfactants play a key role in the synthesis of plasmonic NPs,[33] we hypothesized that supplementing the reaction mixture with DMSO could modify the NPs' morphology. Although DMSO-water mixture have been studied extensively, DMSO has seldom been used in colloidal chemistry.[34-36] For instance, it was used as a solvent and shape-directing agent in order to stabilize the {311} facets of Au bipyramids with an octagonal cross section.[35] In another example, coordination of DMSO to the surface of gold nanorods favored the formation of Au@Ag octahedra.[36]

In this work, silver nanorods (AgNRs) were prepared by overgrowth of Ag onto gold bipyramids (AuBPs). We show that DMSO can be used to break the symmetry of the AgNRs by restricting Ag growth to one side of the AuBP seed. The systematic variation of DMSO concentration in the synthesis was studied, and the effects on the morphology and symmetry of the AgNRs are described. Through experiments and all-atom molecular dynamics (MD) simulations, we show that the adsorption of DMSO significantly changes the chemical

environment of the AuBP surface, leading to the onset of asymmetric growth. In addition, the modification of micelle geometry and the replacement of chloride ions at the gold interface at high DMSO concentration (above 20% (v/v)) induce the growth of silver along the transverse axis of AuBPs. In concert, these results show the potential of DMSO for controlling the morphology and seed-location of AgNRs.

Results and discussion

AuBPs were prepared with a high shape yield by seed-mediated growth from decahedral seeds, as recently reported (**Figure S1**).[7, 37, 38] Ag rods were formed by controlled overgrowth along the fivefold axis of Au bipyramids in the presence of cetyltrimethylammonium chloride (CTAC) and ascorbic acid (AA) at 70°C (**Figure 1A**). In these conditions, centrosymmetric nanostructures were obtained, with the bipyramids located at the center of mass of the AgNRs (**Figure 1B**).

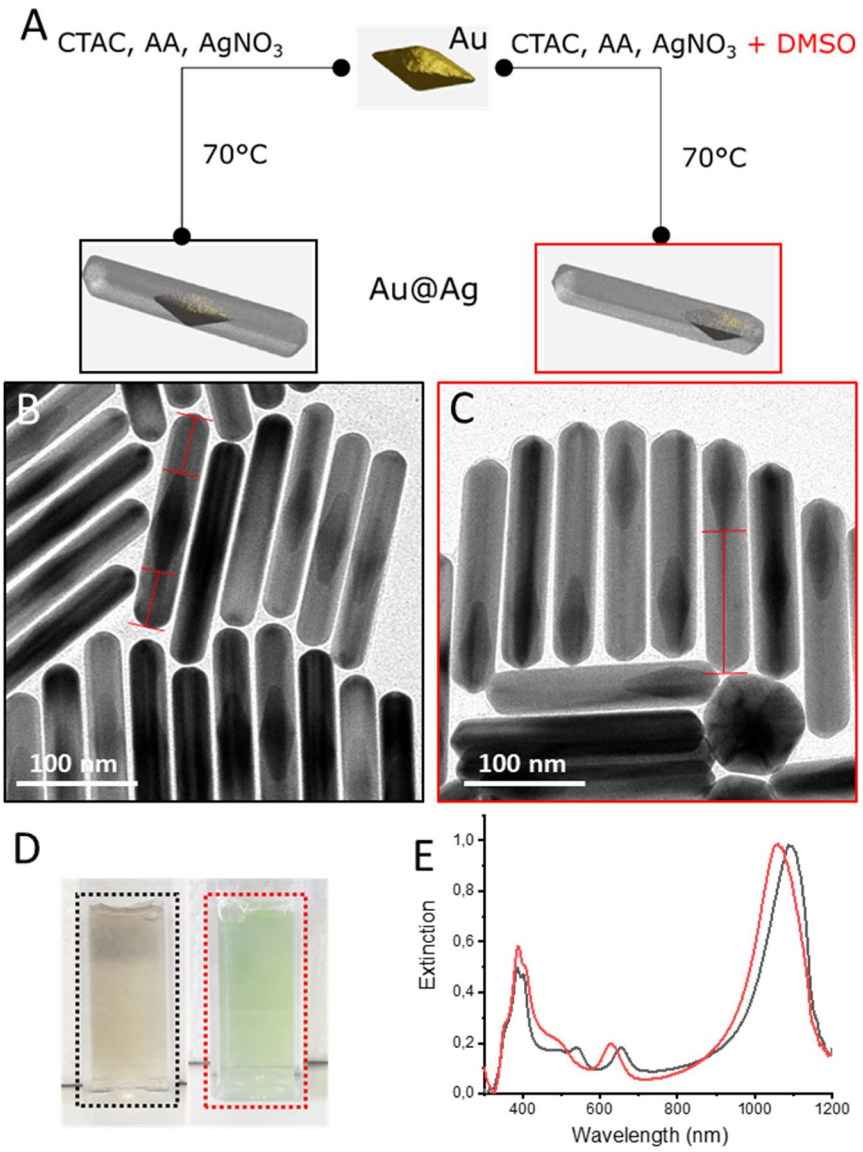

Figure 1: Asymmetric growth of Ag on Au bipyramids in mixed water/DMSO solvents. A) Schematic description of the preparation procedure. B-C) TEM image of symmetric (B) and asymmetric NPs (C) obtained in the absence and presence of DMSO, respectively. In B) Ag rods (186 nm in length and 32 nm in width) were prepared with 3.5 molar equivalent of Ag/Au, whereas in C) the Ag rods (196 nm in length and 35 nm in width) were prepared with 6 molar equivalent of Ag/Au and 5% (v/v) DMSO. D) Photograph of the corresponding dispersions in cuvettes. E) Extinction spectra of the dispersion containing symmetric (black) and asymmetric rods (red).

The inversion symmetry of the AgNR growth was broken when DMSO was used as a co-solvent in the concentration range of 6-10% (v/v) (**Figure 1C**). Its addition significantly modified the growth process, resulting in a new type of nanostructure, in which the bipyramid was located at one end of the AgNR. Although the particle sizes were similar, their optical properties were strikingly different (**Figure 1D**) due to the influence of the asymmetry of the seed placement on the optical shift of the higher-order multipolar modes (**Figure 1E**, **Figure S2**). In order to better understand the NP structure, single NPs were investigated by high-resolution Scanning transmission electron microscopy (STEM) (**Figure 2**).

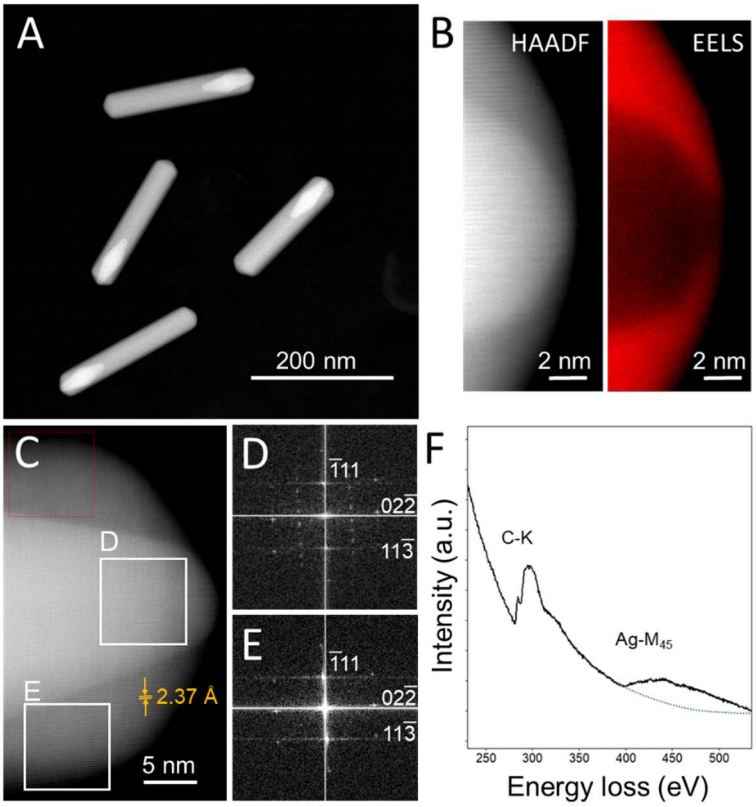

Figure 2: High-resolution and chemical mapping of the asymmetric Ag rods. A) Low-magnification HAADF-STEM image; B) HAADF-STEM image of the tip of Ag rods and the corresponding electron energy loss spectroscopy (EELS) mapping from the silver M45-edge signal (after the subtraction of the background, schematically represented by the dotted blue line). Image and EELS data are collected simultaneously. A typical EELS spectrum is shown in figure (F); C) High resolution HAADF-STEM image. The crystallinity of the silver shell can

be observed in the corresponding Fourier transforms (acquired from the areas labeled as (D) and (E) in panel (C)). The additional spots in D correspond to the superposition of two FCC crystals with different orientation and are characteristic of a pentatwinned nanostructure, as previously described.[39]

STEM high-angle annular dark field (STEM-HAADF) images clearly show the location of the Au seeds at one tip of the Ag rods due to the difference in electron density between Au and Ag (**Figure 2A, Figure S3**). Elemental mapping was performed by electron energy loss spectroscopy (EELS) at the extremity of the Ag rods where the AuBPs are located (**Figure 2B**). This analysis revealed the presence of a few monolayers of silver covering the surface of the AuBP tips at the end of the Ag rods. In some other AgNRs, this silver layer was difficult to detect (**Figure S4**). High-resolution STEM images and the corresponding FFT confirmed the epitaxial relationship between the Au core and the Ag shell, which display the same crystalline orientation in the two regions (**Figure 2 D-E**). In this sense, the crystal structure of asymmetric AgNRs is similar to that reported for symmetric AgNRs.[7]

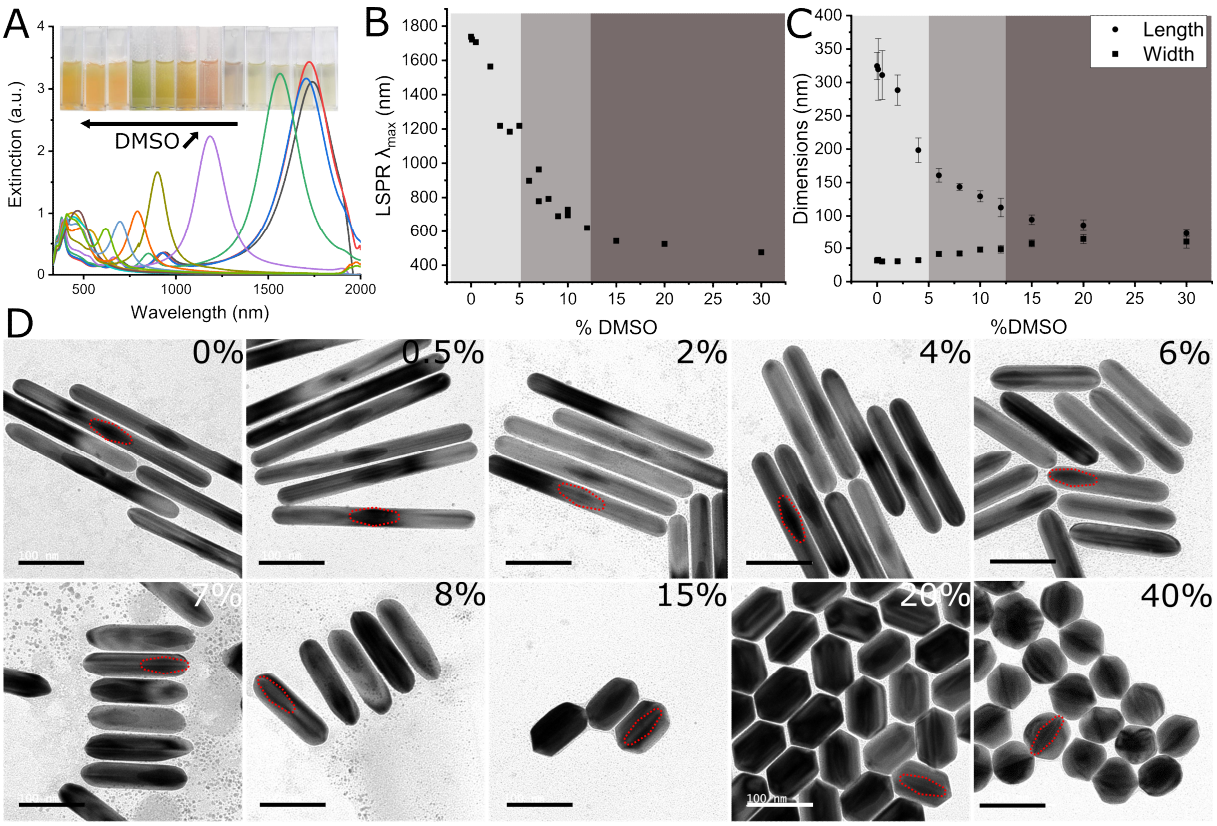

Figure 3: Morphological control by tuning DMSO concentration. A) Extinction spectra of Ag rods synthesized with various DMSO concentrations. The inset shows images of the corresponding dispersions in cuvettes. B) Position of the longitudinal surface plasmon resonance (LSPR) as a function of the DMSO concentration. The three grey-shaded areas denote three different morphologies: symmetric rods (left), asymmetric rods (middle), isotropic NPs (right). C) Size dispersion (length and width) obtained from TEM image analysis of Ag rods for different DMSO concentrations. The grey shades denote NP morphologies as in B). D) Representative TEM images of the Ag rods synthesized with varying DMSO concentration. Scale bars on all images are 100 nm.

The synthesis was then carried out at a DMSO concentration *f* in the range 0-40% (v/v), keeping other experimental parameters fixed, and the resulting NPs were characterized by extinction spectroscopy and TEM (**Figure 3**). Note that *f* could not be increased above 50% (v/v) due to

DMSO-induced colloidal destabilization. Upon increasing *f*, the LSPR was blue shifted from 1800 nm (at *f* = 0%) to 500 nm (at *f* = 30 %), indicating a decrease in aspect ratio for the Ag rods (**Figure 3A-B**). TEM confirmed that the Ag rods shortened (from 325 nm to 72 nm) and thickened (from 30 nm to 60 nm) resulting in nearly isotropic NPs at *f* = 30% (**Figure 3C**). Asymmetric rods were obtained above *f* = 6% and the growth occurred mostly along the transverse axis of the seed above *f* = 20%, as shown by TEM image analysis. The dimensions of the NPs are summarized in **Table S1**. In all cases, the AuBPs were located either at the center of mass or at one end, but very seldom at an intermediate position. We identified three growth regimes, indicated by three shades of grey in **Figure 3-B-C**: (i) longitudinal symmetric growth (*f* between 0-4%), (ii) longitudinal asymmetric growth (*f* between 6-10%) and (iii) transverse symmetric growth (*f* above 20%). Overall, these experiments show that the morphology of the NPs and the symmetry of AgNR growth can be controlled by varying the DMSO concentration.

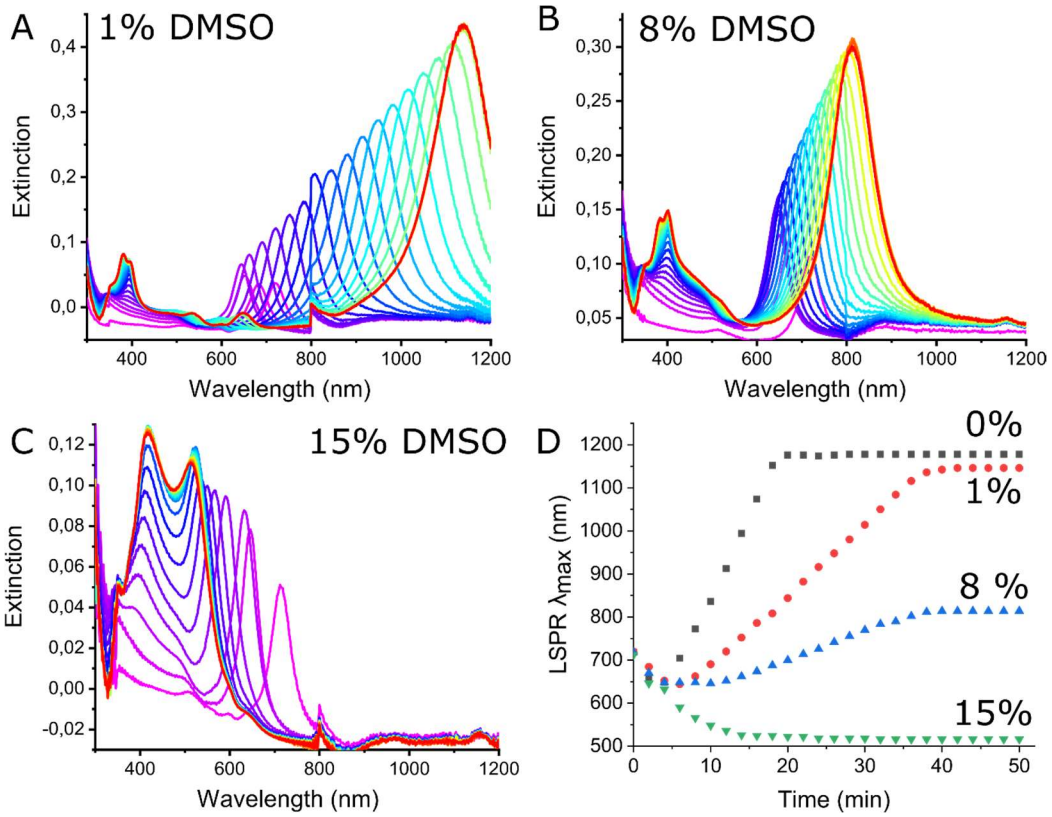

Figure 4: Growth kinetics of the Ag rods in presence of DMSO. A-C) Time-dependent extinction spectra of the Ag nanorods, acquired every 2 min after the addition of the precursor and heating up to 70°C. D) Position of the maximum of the longitudinal LSPR as a function of time of the corresponding growth kinetics.

The growth kinetics of the AgNPs at varying DMSO concentration was followed by *in situ* extinction spectroscopy (**Figure 4**). At $f = 15\%$, the LSPR band blue shifted continuously, indicating that the NPs grew only in the transverse direction (**Figure 4C**), resulting in the more isotropic NPs displayed in **Figure 3D**. The time at which the LSPR stopped evolving was different from sample to sample: 20 minutes, 38 minutes and 40 minutes for $f = 0\%$, 1% and 8%, respectively (**Figure 4D**), showing that DMSO reduced the Ag deposition rate onto the AuBPs.

From the above experiments, it is unclear whether the mechanism of asymmetric growth arises from DMSO adsorption at the AuNP surface, deformation of the CTAC micelles induced by DMSO or a combination of both effects. To better understand the interactions between DMSO and the AuBP surface and their role in the asymmetric growth induced by DMSO in the synthesis of the AgNRs, all-atom molecular dynamics (MD) simulations were performed (**Figure 5**). A CTAC micelle was simulated at the Au (111) surface with DMSO concentrations $f = 0$, 9, and 18%. The Au(111) surface was chosen in lieu of higher-index facets such as (711) that have been observed with AuBPs[40] because the GolP-CHARMM parameters[41] used for gold were shown to accurately reproduce molecular absorption energies compared with nonpolarizable force fields that allow the construction of arbitrary facets.[42] The first observation from these simulations is that the CTAC micelle in water clearly becomes more closely associated with the Au surface over the 150 ns trajectory (**Figure 5A**). In contrast, for $f = 9\%$ DMSO, the distance between the micelle and the Au interface increases over the course of the trajectory, with only a small cluster of CTA^+ molecules remaining associated after 150 ns.

(**Figure 5B**). While a similar effect is observed for f = 18%, in this case the CTAC micelle also assumes an oblate form, somewhat resembling a bilayer patch by 150 ns (**Figure S6**). In line with this observation, previous experiments have shown that DMSO disrupts the formation of CTAB micelles, which is likely the cause of isotropic growth observed at f = 18% and above.[32]

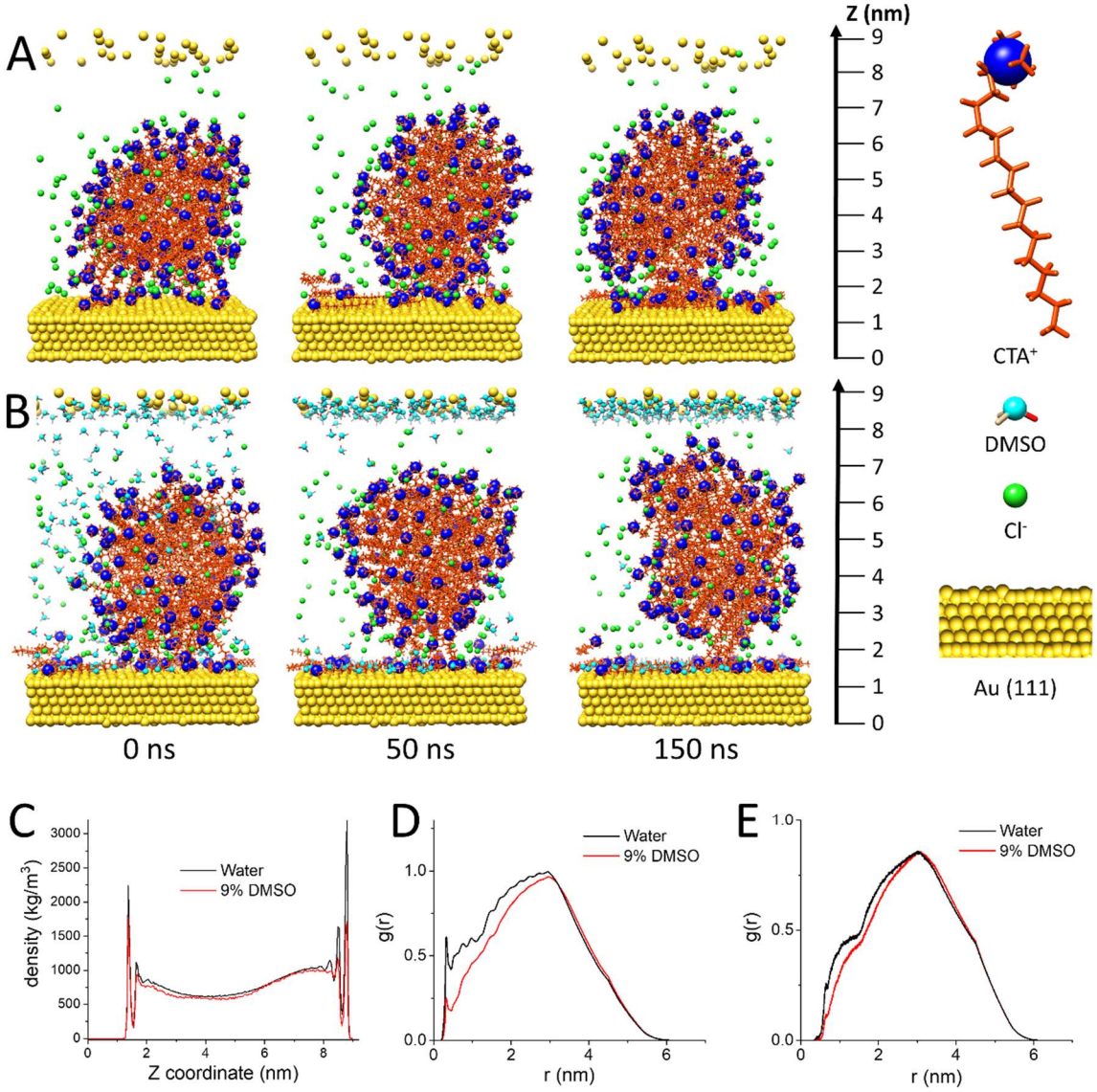

Figure 5. All-atom molecular dynamics simulations of CTAC micelles interacting with Au(111) in A) water; B) 9% (v/v) DMSO in water. C) Density of water molecules along the z-axis of the simulation box; Radial distribution functions showing the relative distance distribution of Au(111) surface atoms with D) water molecules and E) Cl^- ions.

To better understand the influence of DMSO adsorption on interactions between the Au(111) surface and Cl^-, Water, DMSO, CTA^+, and the N^+ of CTA, their densities, as well as the radial distribution functions (RDF) between these groups and the surface Au atoms, were calculated. One effect that is clearly observed is the loss of structured water at the interface. Comparing the density plots of water revealed that both the amount of interfacial water and its degree of long-range order decreased with increasing *f* (**Figure 5C**). For *f* = 0% there were four distinct layers of structured interfacial water, whereas for *f* = 9% and 18% only two remained. The orientation of interfacial water was further investigated by calculating its tetrahedral order parameter, which is defined as the angle (θ) between the dipole moment of water and the normal axis (z).[43] The calculated order parameter (cos (θ)) at the interface opposite the CTAC micelle shows that while there is loss of the typical structure of interfacial water, there is an increase in the ordering of water molecules adjacent to DMSO at the interface (**Figure S7A**). This is likely facilitated by the formation of hydrogen bonds between water and DMSO. The adsorption of DMSO at the Au(111) interface occurs preferentially via the sulfur atom, as clearly demonstrated by the density profile of C, O, and S atoms at the Au(111) interface opposite the micelle over 140 ns (**Figure S7B**). Furthermore, the overall decrease of the amount of water bound to the interface is significant, with about 5 times fewer waters interacting with the Au interface at *f* = 18% compared with *f* = 0%. This can also be clearly observed in the RDF of water with the surface atoms of the Au(111) surface, where increased DMSO leads to decreased likelihood of interaction (**Figure 5D**).

While snapshots of the simulation trajectories suggest that DMSO adsorption onto gold leads to reduced interactions between CTAC micelles and the Au(111) surface, it is known that the binding of CTAC at the gold interface is aided by binding of Cl^- at the interface.[44] Interestingly, the interactions between Cl^- ions and the Au(111) interface were shown to significantly decrease in the presence of DMSO (**Figure 5E**). As these interactions are known to facilitate

the binding of CTAC micelles, such a reduction of Cl^- at the interface may indeed alter the growth kinetics. As DMSO has been reported to alter surfactant micelle formation, the oblate micelles observed at 18% (v/v) in addition to the dissociation of the micelle from the gold interface may provide an explanation for the change in AgNR morphology with increasing DMSO above 15% (**Figure 3**).

The MD simulations provided crucial information about how the interactions between DMSO and the gold interface lead to the displacement of CTA^+ and Cl^-. Additional experiments were performed in order to further verify these effects on the synthesis. To study the replacement of CTA^+ and Cl^- at the interface, the AgNRs were etched in the presence of DMSO, H_2O_2, $NH_3.H_2O$ and CTAC.[12] Without DMSO, anisotropic oxidation through the tips was observed due to the capping of the side facets by CTA^+ and Cl^- as previously reported.[12] However, the side facets were etched in the presence of DMSO, showing that they were no longer passivated (**Figure S8**). This experiment demonstrates that capping agents were replaced by DMSO at the NP surface. In order to experimentally confirm DMSO adsorption on the gold seed, the seeds were incubated with DMSO and centrifuged two times to remove all free DMSO. When the reaction was performed on the day of the purification, asymmetric AgNRs were obtained with the same morphology as the reference sample synthesized in the presence of 5% DMSO (**Figure S9**). However, when the same reaction was performed 44 days after purification, symmetric AgNRs were obtained with the same morphology as the reference sample performed without DMSO (**Figure S9**). This set of experiments demonstrates that DMSO indeed adsorbs onto the gold seeds and that it can desorb upon dilution. Overall, the experiments and MD simulations support DMSO adsorption accompanied by the displacement of CTAC ligands at the NP surface.

Among other strategies, the symmetry of seeded growth can be broken by slowing down the reaction kinetics, either by precursor scarcity, or by surface passivation.[24, 45] The latter

effect explains our findings, as DMSO hinders Ag deposition onto the gold surface. Explanations involving modified reactivity of ionic (i.e. AgCl) and molecular species (i.e. ascorbic acid) by DMSO can be rejected since asymmetric growth is also observed in the presence of only bound DMSO (**Figure S9**). It has been recently suggested that a thin silver coating at the AuBP surface promotes symmetric growth, since asymmetric AgNRs were obtained with Ag-free NPs.[14] In this work, the asymmetric growth cannot be attributed to a possible depletion of the silver layer from the AuBPs surface by DMSO, because symmetric AgNRs can be obtained after incubation with DMSO (**Figure S9**).

Additional experiments were performed without DMSO, but with a syringe pump to control the supply of atoms at the seed surface. Symmetric AgNRs were obtained in the normal procedure (one-shot) and at high injection rate whereas smaller and symmetric AgNRs were obtained at an injection rate in which the reactants were supplied over 5h (**Figure S10**). Asymmetric AgNRs were only obtained in presence of DMSO. While slow kinetics are important to break the symmetry of a seed, it is not the only effect at play explaining the asymmetric growth pattern induced by DMSO. The passivation of the surface by DMSO is also important for the asymmetric longitudinal growth that is observed from a concentration of DMSO (*f* between 5-10%), at which the AuBP surface is presumably capped by DMSO, leaving a few unprotected sites for nucleation and growth. This would confine Ag deposition to a few nucleation sites and favor asymmetric growth. At higher DMSO concentration (*f* above 20%), transverse growth is observed because of the replacement of chloride ions at the gold interface and the deformation of the CTAC micelles. Indeed, when overgrowth was performed after incubation with high DMSO concentration (f = 20%) but after removing free DMSO by centrifugation (in order to limit micelle deformation), transverse growth was limited and asymmetric AgNRs were obtained (**Figure S9**).

Asymmetric growth induced by DMSO was explored on other types of pentatwinned Au seeds. Bimetallic NPs were prepared by overgrowing Ag on pentatwinned AuNRs. The formation of asymmetric nanostructures was also observed for AuNRs, but at higher DMSO content than for AuBPs (**Figure S11**). This experiment shows that this synthetic method is not limited to AuBPs and can be extended to other AuNP morphologies.

Finally, the eventual role of impurities in DMSO on the directed growth of the Ag rods on the AuBPs seed was investigated. Although a DMSO batch with a purity above 99.9% was used, impurities such as dimethyl sulfide (DMS) were also present at a concentration around 0.5 mM,[46] corresponding to a range of 0-0.2 mM in the reaction medium (DMSO concentrations between 0-40%). The synthesis was performed in the presence of DMS concentrations ranging from 0 to 10 mM (**Figure S12**) and a modification of the shape of the Au@Ag rods was noticed, but only for 10 mM DMS. Although DMS does influence the growth of Ag on Au at this relatively high concentration, we conclude that it has a negligible effect in the experiments presented in the manuscript, since the estimated DMS concentration at 6% v/v DMSO is of the order of 30 μM, 333 times lower than the 10 mM necessary to observe an effect of DMS on the growth of the NPs. Additionally, the possible role of impurities in DMSO was investigated by performing the reaction with an old (more than a decade) DMSO batch and comparing the results with those obtained with the fresh batch used in this study. The concentration of the old DMSO batch had to be increased significantly (e.g. 30% instead of 6%) to found non-centrosymmetric NPs. This experiment suggests that DMSO plays a primary role in the asymmetric growth of the Ag rod and that the oxidation products of DMSO have no or only little influence in this respect. Additional experiment with dimethyl sulfone (DMSOO), a known oxidation product of DMSO, were performed in order to confirm this statement. All particles prepared in presence DMSOO, even at concentrations up to 1M, were centrosymmetric

and had similar dimensions compared to the reference sample prepared without DMSOO (**Figure S13**).

Conclusion

A simple, yet robust approach to promote asymmetric growth of Ag on AuBPs was achieved by the addition of DMSO to an aqueous reaction medium. The volume fraction *f* of DMSO was systematically varied and its influence on the morphology and symmetry of the AgNRs was described. We identified 3 growth regimes: (i) longitudinal symmetric growth (*f* between 0-4%), (ii) longitudinal asymmetric growth (*f* between 6-10%) and (iii) transverse symmetric growth (*f* above 20%). Experiments showed that DMSO replaces the capping agent at the NP surface and decreases the Ag deposition rate. In order to better understand the molecular interactions at the gold interface under synthesis conditions, all-atom MD simulations were performed which showed a significant modification of the chemical environment of the Au surface: DMSO strongly binds to the Au(111) interface, displacing interfacial water and reducing its long-range structure, while also reducing the interactions between both Cl^- ions and CTAC micelles with the Au interface. Longitudinal asymmetric growth is induced by DMSO adsorption which influence Ag reduction kinetics while transverse growth is induced by alteration of the CTAC micelle geometry at high DMSO content. In addition to establishing a simple, colloidal approach for asymmetric AgNR growth, this work gives new perspectives for the study of the physical properties of asymmetric NPs. Furthermore, this work shows the potential of DMSO in controlling the synthesis of complex nanostructures and tailoring their linear and nonlinear optical properties, which will advance applications in multimetallic photocatalysis and chemical sensing, to name a few.

Experimental section

Materials. Gold chloride trihydrate ($HAuCl_4.3H_2O$ ≥99.9%), silver nitrate ($AgNO_3$ >99%), hydrochloric acid (HCl 37%), sodium borohydride ($NaBH_4$ ≥96%), L-ascorbic acid (≥99%), anhydrous dimethylsulfoxyde (DMSO ≥99.9%), cetyltrimethylammonium bromide (CTAB ≥99%), cetyltrimethylammonium chloride (CTAC 25wt% in H_2O) and benzyldimethylhexadecylammonium chloride (BDAC 99%) were purchased from Merck.

Bipyramids synthesis and purification. AuBPs were synthesized as described previously.[37, 38, 47] Briefly, 2 mL of $AgNO_3$ 10 mM, 4 mL of $HAuCl_4$ 25 mM and 4 mL of HCl 1 M were added in 200 mL of CTAB 100 mM. Then, 1600 µL of ascorbic acid 100 mM were added, followed by 3600 µL of seeds.[7] After 4 hours at 30°C, the bipyramids were centrifuged twice and purified by depletion during one night at 30°C in BDAC 350 mM.[48] The supernatant was removed, the precipitate was redispersed in water and washed twice with CTAC 10 mM. The AuBPs were finaly redispersed in 2 mL of CTAC 10 mM.

Silver growth procedure. For every growth procedure, the overall volume was fixed to 2 mL by adjusting the quantity of water. The gold concentration was 0.25 mM, the CTAC concentration was 10 mM. In a typical synthesis, 200 µL of CTAC 100 mM, 100 µL of DMSO and 43.2 µL of AuBPs ($n_{Au} = 5.10^{-7}$ mol) were added to 1632 µL of water. The mixture was stirred in an oil bath at 70°C for 20 minutes and 25 µL of $AgNO_3$ 100 mM was added, immediately followed by 100 µL of ascorbic acid 100 mM. The reaction medium was left under stirring at 70°C for 2 hours. AgNRs were then washed two times by centrifugation and pellet redispersion in water before TEM observation.

Characterization of the nanoparticles. UV/Vis/NIR absorption spectra were collected using a Cary 5000 UV-Vis-NIR. All experiments were carried out at room temperature, using disposable polystyrene cuvettes with optical paths of 1 cm. TEM was performed at IMAGIF (*I2BC* CNRS, Gif s/Yvette, France) using a JEOL JEM-1400 microscope operating at 120 kV

with a filament current of about 55 µA. High resolution HAADF images and EELS data were recorded using a Nion UltraSTEM 200 operating at 100 kV, equipped with a spherical aberration corrector and a High-Angle Annular Dark-Field (HAADF) detector with an inner collection angle of 70 mrad. Core-loss EELS spectra were acquired with an energy dispersion of 0.5 eV/channel in the energy range corresponding to the Ag M_{45}-edge. Spectra were recorded in the spectrum imaging mode, *i.e.* the focused electron probe is scanned, step by step, over the region of interest and a whole spectrum is acquired at each position. A typical hyperspectral image contains about 20000 spectra. Data were denoised by using as a filtering method, principal component analysis (PCA) under Hyperspy, an open-source software suite (http://hyperspy.org/, DOI: 10.5281/zenodo.4294676). Elemental maps corresponding to silver distribution in NRs were obtained from EELS data by integrating the Ag signal after background subtraction in front of the respective edge.

Molecular Dynamics Simulations. MD simulations and analysis were carried out using GROMACS 2020.[49] The GolP-CHARMM forcefield was used to describe the Au (111) surface.[41] The GolP-CHARMM forcefield provides dynamic polarization through the use of two virtual sites offset from each gold atom with partial charges of +0.3 and -0.3, respectively. This provides more accurate depictions of the surface binding interactions of small molecules with the Au surface than models which rely solely on the use of Lennard-Jones (LJ) terms. DMSO and CTA^+ were modeled using the CHARMM36 forcefield, as described in previous studies.[50, 51] Parameters for Cl^- were derived from Joung and Cheatham, and the TIP3P water model was used.[52, 53] Additional simulation details are given in the supporting information.

Associated content

Supporting Information

Details about MD simulations, other TEM, HRTEM and MD simulations results. This material is available free of charge via the Internet at http://pubs.acs.org.

Author information

Corresponding authors

***E-mail:** eric.hill@chemie.uni-hamburg.de

***E-mail:** doru.constantin@universite-paris-saclay.fr

***E-mail:** cyrille.hamon@universite-paris-saclay.fr

Acknowledgements

The CNRS is acknowledged for funding and support. The present work has benefited from the electronic microscopy facility of Imagerie-Gif, (***http://www.i2bc.paris-saclay.fr***), member of IBiSA (http://www.ibisa.net), supported by "France-BioImaging" (*ANR-10-INBS-04-01*), and the Labex "Saclay Plant Science" (*ANR-11-IDEX-0003-02*). We thank Debi Evans at the University of New Mexico for providing computing resources. E.H.H. is supported by the Cluster of Excellence 'Advanced Imaging of Matter' of the Deutsche Forschungsgemeinschaft (DFG) - EXC 2056 - project ID 390715994. This project has also received funding from the European Union's Horizon 2020 Research and innovation programme under grant agreement N° 823717.

References

1. Huang, X.; Neretina, S.; El-Sayed, M. A., Gold Nanorods: From Synthesis and Properties to Biological and Biomedical Applications. *Adv. Mater.* **2009,** 21, (48), 4880-4910.

2. Xia, Y.; Gilroy, K. D.; Peng, H. C.; Xia, X., Seed-Mediated Growth of Colloidal Metal Nanocrystals. *Angew. Chem. Int. Ed.* **2017,** 56, (1), 60-95.

3. Murphy, C. J.; Jana, N. R., Controlling the Aspect Ratio of Inorganic Nanorods and Nanowires. *Adv. Mater.* **2002,** 14, (1), 80-82.

4. Sun, Y.; Gates, B.; Mayers, B.; Xia, Y., Crystalline Silver Nanowires by Soft Solution Processing. *Nano Lett.* **2002,** 2, (2), 165-168.

5. Lofton, C.; Sigmund, W., Mechanisms Controlling Crystal Habits of Gold and Silver Colloids. *Adv. Funct. Mater.* **2005,** 15, (7), 1197-1208.

6. Huo, D.; Kim, M. J.; Lyu, Z.; Shi, Y.; Wiley, B. J.; Xia, Y., One-Dimensional Metal Nanostructures: From Colloidal Syntheses to Applications. *Chem. Rev.* **2019,** 119, (15), 8972-9073.

7. Aliyah, K.; Lyu, J.; Goldmann, C.; Bizien, T.; Hamon, C.; Alloyeau, D.; Constantin, D., Real-Time In Situ Observations Reveal a Double Role for Ascorbic Acid in the Anisotropic Growth of Silver on Gold. *J. Phys. Chem. Lett.* **2020,** 11, (8), 2830-2837.

8. Gómez-Graña, S.; Goris, B.; Altantzis, T.; Fernández-López, C.; Carbó-Argibay, E.; Guerrero-Martínez, A.; Almora-Barrios, N.; López, N.; Pastoriza-Santos, I.; Pérez-Juste, J.; Bals, S.; Van Tendeloo, G.; Liz-Marzán, L. M., Au@Ag Nanoparticles: Halides Stabilize {100} Facets. *J. Phys. Chem. Lett.* **2013,** 4, (13), 2209-2216.

9. Okuno, Y.; Nishioka, K.; Kiya, A.; Nakashima, N.; Ishibashi, A.; Niidome, Y., Uniform and controllable preparation of Au-Ag core-shell nanorods using anisotropic silver shell formation on gold nanorods. *Nanoscale* **2010,** 2, (8), 1489-1493.

10. Park, K.; Drummy, L. F.; Vaia, R. A., Ag shell morphology on Au nanorod core: role of Ag precursor complex. *J. Mater. Chem.* **2011,** 21, (39), 15608-15618.

11. Hamon, C.; Goldmann, C.; Constantin, D., Controlling the symmetry of supercrystals formed by plasmonic core–shell nanorods with tunable cross-section. *Nanoscale* **2018,** 10, (38), 18362-18369.

12. Zhuo, X.; Zhu, X.; Li, Q.; Yang, Z.; Wang, J., Gold Nanobipyramid-Directed Growth of Length-Variable Silver Nanorods with Multipolar Plasmon Resonances. *ACS nano* **2015,** 9, (7), 7523-35.

13. Mayer, M.; Scarabelli, L.; March, K.; Altantzis, T.; Tebbe, M.; Kociak, M.; Bals, S.; García de Abajo, F. J.; Fery, A.; Liz-Marzán, L. M., Controlled Living Nanowire Growth: Precise Control over the Morphology and Optical Properties of AgAuAg Bimetallic Nanowires. *Nano Lett.* **2015,** 15, (8), 5427-5437.

14. Sánchez-Iglesias, A.; Zhuo, X.; Albrecht, W.; Bals, S.; Liz-Marzán, L. M., Tuning Size and Seed Position in Small Silver Nanorods. *ACS Mater. Lett.* **2020**, 1246-1250.

15. Chow, T. H.; Li, N.; Bai, X.; Zhuo, X.; Shao, L.; Wang, J., Gold Nanobipyramids: An Emerging and Versatile Type of Plasmonic Nanoparticles. *Acc. Chem. Res.* **2019,** 52, (8), 2136-2146.

16. Zhuo, X.; Yip, H. K.; Ruan, Q.; Zhang, T.; Zhu, X.; Wang, J.; Lin, H. Q.; Xu, J. B.; Yang, Z., Broadside Nanoantennas Made of Single Silver Nanorods. *ACS nano* **2018,** 12, (2), 1720-1731.

17. Liu, J.; Zhang, J., Nanointerface Chemistry: Lattice-Mismatch-Directed Synthesis and Application of Hybrid Nanocrystals. *Chem. Rev.* **2020,** 120, (4), 2123-2170.

18. Cathcart, N.; Kitaev, V., Symmetry Breaking by Surface Blocking: Synthesis of Bimorphic Silver Nanoparticles, Nanoscale Fishes and Apples. *Sci. Rep.* **2016,** 6, 32561.

19. Huang, J.; Zhu, Y.; Liu, C.; Shi, Z.; Fratalocchi, A.; Han, Y., Unravelling Thiol's Role in Directing Asymmetric Growth of Au Nanorod–Au Nanoparticle Dimers. *Nano Lett.* **2016,** 16, (1), 617-623.

20. Huang, Z.; Gong, J.; Nie, Z., Symmetry-Breaking Synthesis of Multicomponent Nanoparticles. *Acc. Chem. Res.* **2019,** 52, (4), 1125-1133.

21. Rodriguez-Fernandez, D.; Altantzis, T.; Heidari, H.; Bals, S.; Liz-Marzan, L. M., A protecting group approach toward synthesis of Au-silica Janus nanostars. *Chem. Comm.* **2014,** 50, (1), 79-81.

22. Wang, F.; Cheng, S.; Bao, Z.; Wang, J., Anisotropic Overgrowth of Metal Heterostructures Induced by a Site-Selective Silica Coating. *Angew. Chem. Int. Ed.* **2013,** 52, (39), 10344-10348.

23. Qiu, J.; Xie, M.; Lyu, Z.; Gilroy, K. D.; Liu, H.; Xia, Y., General Approach to the Synthesis of Heterodimers of Metal Nanoparticles through Site-Selected Protection and Growth. *Nano Lett.* **2019,** 19, (9), 6703-6708.

24. Xia, Y.; Xia, X.; Peng, H. C., Shape-Controlled Synthesis of Colloidal Metal Nanocrystals: Thermodynamic versus Kinetic Products. *J. Am. Chem. Soc.* **2015,** 137, (25), 7947-66.

25. Personick, M. L.; Mirkin, C. A., Making sense of the mayhem behind shape control in the synthesis of gold nanoparticles. *J. Am. Chem. Soc.* **2013,** 135, (49), 18238-47.

26. Zeng, J.; Zhu, C.; Tao, J.; Jin, M.; Zhang, H.; Li, Z.-Y.; Zhu, Y.; Xia, Y., Controlling the Nucleation and Growth of Silver on Palladium Nanocubes by Manipulating the Reaction Kinetics. *Angew. Chem. Int. Ed.* **2012,** 51, (10), 2354-2358.

27. Lv, T.; Yang, X.; Zheng, Y.; Huang, H.; Zhang, L.; Tao, J.; Pan, L.; Xia, Y., Controlling the Growth of Au on Icosahedral Seeds of Pd by Manipulating the Reduction Kinetics. *J. Phys. Chem. C* **2016,** 120, (37), 20768-20774.

28. Yang, Y.; Wang, W.; Li, X.; Chen, W.; Fan, N.; Zou, C.; Chen, X.; Xu, X.; Zhang, L.; Huang, S., Controlled Growth of Ag/Au Bimetallic Nanorods through Kinetics Control. *Chem. Mater.* **2013,** 25, (1), 34-41.

29. Alfassi, Z. B.; Filby, W. G., The question of micelle formation in non-aqueous polar solvents: Positron annihilation results. *Chem. Phys. Lett.* **1988,** 144, (1), 83-86.

30. Peyre, V.; Bouguerra, S.; Testard, F., Micellization of dodecyltrimethylammonium bromide in water–dimethylsulfoxide mixtures: A multi-length scale approach in a model system. *J. Colloid Interface Sci.* **2013,** 389, (1), 164-174.

31. Singh, H. N.; Saleem, S. M.; Singh, R. P.; Birdi, K. S., Micelle formation of ionic surfactants in polar nonaqueous solvents. *J. Phys. Chem.* **1980,** 84, (17), 2191-2194.

32. Ionescu, L. G.; Tokuhiro, T.; Czerniawski, B. J.; Smith, E. S., Formation of Micelles of Cetyltrimethylammonium Bromide in Water-Dimethyl Sulfoxide Solutions. In *Solution Chemistry of Surfactants: Volume 1*, Mittal, K. L., Ed. Springer New York: Boston, MA, 1979; pp 487-496.

33. González-Rubio, G.; Scarabelli, L.; Guerrero-Martínez, A.; Liz-Marzán, L. M., Surfactant-Assisted Symmetry Breaking in Colloidal Gold Nanocrystal Growth. *ChemNanoMat* **2020,** 6, (5), 698-707.

34. Nishida, K.; Kawasaki, H., Effective removal of surface-bound cetyltrimethylammonium ions from thiol-monolayer-protected Au nanorods by treatment with dimethyl sulfoxide/citric acid. *RSC Adv.* **2017,** 7, (29), 18041-18045.

35. Niu, W.; Duan, Y.; Qing, Z.; Huang, H.; Lu, X., Shaping Gold Nanocrystals in Dimethyl Sulfoxide: Toward Trapezohedral and Bipyramidal Nanocrystals Enclosed by {311} Facets. *J. Am. Chem. Soc.* **2017,** 139, (16), 5817-5826.

36. Haidar, I.; Day, A.; Decorse, P.; Lau-Truong, S.; Chevillot-Biraud, A.; Aubard, J.; Félidj, N.; Boubekeur-Lecaque, L., Tailoring the Shape of Anisotropic Core–Shell Au–Ag Nanoparticles in Dimethyl Sulfoxide. *Chem. Mater.* **2019,** 31, (8), 2741-2749.

37. Chateau, D.; Liotta, A.; Vadcard, F.; Navarro, J. R.; Chaput, F.; Lerme, J.; Lerouge, F.; Parola, S., From gold nanobipyramids to nanojavelins for a precise tuning of the plasmon resonance to the infrared wavelengths: experimental and theoretical aspects. *Nanoscale* **2015,** 7, (5), 1934-43.

38. Sanchez-Iglesias, A.; Winckelmans, N.; Altantzis, T.; Bals, S.; Grzelczak, M.; Liz-Marzan, L. M., High-Yield Seeded Growth of Monodisperse Pentatwinned Gold Nanoparticles through Thermally Induced Seed Twinning. *J. Am. Chem. Soc.* **2017,** 139, (1), 107-110.

39. Johnson, C. J.; Dujardin, E.; Davis, S. A.; Murphy, C. J.; Mann, S., Growth and form of gold nanorods prepared by seed-mediated, surfactant-directed synthesis. *J. Mater. Chem.* **2002,** 12, (6), 1765-1770.

40. Liu; Guyot-Sionnest, P., Mechanism of Silver(I)-Assisted Growth of Gold Nanorods and Bipyramids. *J. Phys. Chem. B* **2005,** 109, (47), 22192-22200.

41. Wright, L. B.; Rodger, P. M.; Corni, S.; Walsh, T. R., GolP-CHARMM: First-Principles Based Force Fields for the Interaction of Proteins with Au(111) and Au(100). *J. Chem. Theory Comput.* **2013,** 9, (3), 1616-1630.

42. Heinz, H.; Lin, T.-J.; Kishore Mishra, R.; Emami, F. S., Thermodynamically Consistent Force Fields for the Assembly of Inorganic, Organic, and Biological Nanostructures: The INTERFACE Force Field. *Langmuir* **2013,** 29, (6), 1754-1765.

43. Chau, P. L.; Hardwick, A. J., A new order parameter for tetrahedral configurations. *Mol. Phys.* **1998,** 93, (3), 511-518.

44. Meena, S. K.; Celiksoy, S.; Schäfer, P.; Henkel, A.; Sönnichsen, C.; Sulpizi, M., The role of halide ions in the anisotropic growth of gold nanoparticles: a microscopic, atomistic perspective. *Phys. Chem. Chem. Phys.* **2016,** 18, (19), 13246-13254.

45. Gilroy, K. D.; Peng, H.-C.; Yang, X.; Ruditskiy, A.; Xia, Y., Symmetry breaking during nanocrystal growth. *Chem. Commun.* **2017,** 53, (33), 4530-4541.

46. Garusinghe, G. S. P.; Bessey, S. M.; Boyd, C.; Aghamoosa, M.; Frederick, B. G.; Bruce, M. R. M.; Bruce, A. E., Identification of dimethyl sulfide in dimethyl sulfoxide and implications for metal-thiolate disulfide exchange reactions. *RSC Adv.* **2015,** 5, (51), 40603-40606.

47. Li, X.; Lyu, J.; Goldmann, C.; Kociak, M.; Constantin, D.; Hamon, C., Plasmonic Oligomers with Tunable Conductive Nanojunctions. *J. Phys. Chem. Lett.* **2019,** 10, (22), 7093-7099.

48. Lee, J. H.; Gibson, K. J.; Chen, G.; Weizmann, Y., Bipyramid-templated synthesis of monodisperse anisotropic gold nanocrystals. *Nat. Commun.* **2015,** 6, 7571.

49. Abraham, M. J.; Murtola, T.; Schulz, R.; Páll, S.; Smith, J. C.; Hess, B.; Lindahl, E., GROMACS: High performance molecular simulations through multi-level parallelism from laptops to supercomputers. *SoftwareX* **2015,** 1-2, 19-25.

50. Huang, J.; MacKerell Jr, A. D., CHARMM36 all-atom additive protein force field: Validation based on comparison to NMR data. *J. Comput. Chem.* **2013,** 34, (25), 2135-2145.

51. Hanske, C.; Hill, E. H.; Vila-Liarte, D.; González-Rubio, G.; Matricardi, C.; Mihi, A.; Liz-Marzán, L. M., Solvent-Assisted Self-Assembly of Gold Nanorods into Hierarchically Organized Plasmonic Mesostructures. *ACS Appl. Mater. Interfaces* **2019,** 11, (12), 11763-11771.

52. Joung, I. S.; Cheatham, T. E., Determination of Alkali and Halide Monovalent Ion Parameters for Use in Explicitly Solvated Biomolecular Simulations. *J. Phys. Chem. B* **2008,** 112, (30), 9020-9041.

53. Stillinger, F. H.; Rahman, A., Improved simulation of liquid water by molecular dynamics. *J. Chem. Phys.* **1974,** 60, (4), 1545-1557.

TOC Graphic